Title
Contribution of Organic Nitrates to Organic Aerosol over South Korea during KORUS-AQ

Journal
Environmental Science and Technology, 55(24)

ISSN
0013-936X

Authors
Kenagy, Hannah S
Present, Paul S Romer
Wooldridge, Paul J
et al.

Publication Date
2021-12-21

DOI
10.1021/acs.est.1c05521

Peer reviewed

Published in final edited form as:
Environ Sci Technol. 2021 December 21; 55(24): 16326–16338. doi:10.1021/acs.est.1c05521.

Contribution of organic nitrates to organic aerosol over South Korea during KORUS-AQ

Hannah S. Kenagy[†], **Paul S. Romer Present**[†,††], **Paul J. Wooldridge**[†], **Benjamin A. Nault**[‡,¶,‡‡], **Pedro Campuzano-Jost**[‡,¶], **Douglas A. Day**[‡,¶], **Jose L. Jimenez**[‡,¶], **Azimeh Zare**[§], **Havala O.T. Pye**[‖], **Jinhyeok Yu**[⊥], **Chul H. Song**[⊥], **Donald R. Blake**[#], **Jung-Hun Woo**[@], **Younha Kim**[△], **Ronald C. Cohen**[†,▽]

[†]Department of Chemistry, University of California, Berkeley, CA 94720, USA

[‡]Department of Chemistry, University of Colorado, Boulder, CO 80309, USA

[¶]Cooperative Institute for Research in Environmental Sciences, University of Colorado, Boulder, CO 80309, USA

[§]Department of Chemistry, University of California, Berkeley, CA 94710, USA

[‖]Office of Research and Development, US Environmental Protection Agency, Research Triangle Park, NC 27709, United States

[⊥]School of Earth Sciences and Environmental Engineering, Gwangju Institute of Science and Technology (GIST), Gwangju 61105, Republic of Korea

[#]Department of Chemistry, University of California, Irvine, CA 92697, USA

[@]Department of Civil and Environmental Engineering, Konkuk University, Seoul 05029, Republic of Korea

[△]Energy, Climate, and Environment (ECE) Program, International Institute for Applied Systems Analysis (IIASA), Laxenburg A-2361, Austria

[▽]Department of Earth Planetary Sciences, University of California, Berkeley, CA 94720, USA

[††]Now at: Colorado Department of Public Health and Environment, Denver, CO 80246, USA

[‡‡]Now at: Center for Aerosol and Cloud Chemistry, Aerodyne Research, Inc., Billerica, MA 01821, USA

Abstract

The role of anthropogenic NO_x emissions in secondary organic aerosol (SOA) production is not fully understood but is important for understanding the contribution of emissions to air quality. Here, we examine the role of organic nitrates ($RONO_2$) in SOA formation over the Korean Peninsula during the KORUS-AQ field study in spring 2016 as a model for $RONO_2$ aerosol in

rccohen@berkeley.edu .

Supporting Information Available

Particle loss corrections applied to TD-LIF measurements, CU-AMS measurements of $pRONO_2$, comparison of TD-LIF and CU-AMS $pRONO_2$ measurements, CU-AMS measurements of OA, WAS measurements of VOCs, comparison of OH and Cl oxidation of VOCs, CMAQ emissions, model-measurements comparison, and CMAQ-modeled $RONO_2$ speciation.

cities worldwide. We use aircraft-based measurements of particle-phase and total (gas + particle) $RONO_2$ to explore $RONO_2$ phase partitioning. These measurements show that, on average, 1/4 of $RONO_2$ are in the condensed phase, and we estimate that ≈15% of the organic aerosol (OA) mass can be attributed to $RONO_2$. Further, we observe that the fraction of $RONO_2$ in the condensed phase increases with OA concentration, evidence that equilibrium absorptive partitioning controls the $RONO_2$ phase distribution. Lastly, we model $RONO_2$ chemistry and phase partitioning in the CMAQ chemical transport model. We find that known chemistry can account for 1/3 of the observed $RONO_2$, but there is a large missing source of semi-volatile, anthropogenically-derived $RONO_2$. We propose this missing source may result from oxidation of semi- and intermediate-volatility organic compounds and/or from anthropogenic molecules that undergo autoxidation or multiple generations of OH-initiated oxidation.

Graphical Abstract

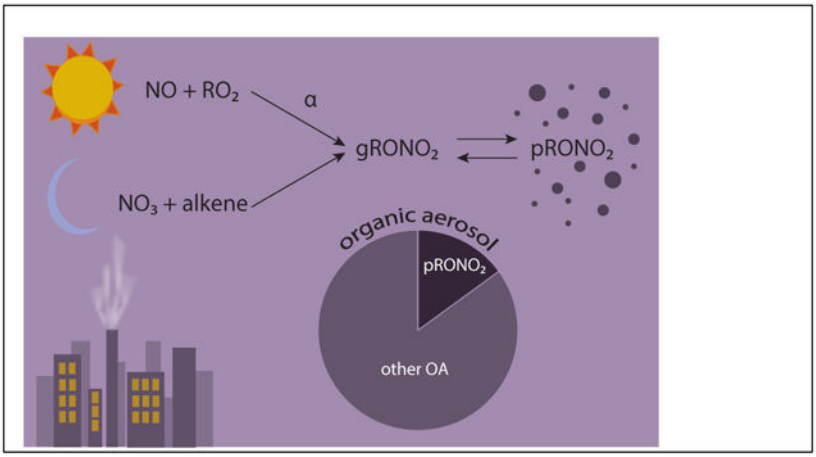

Keywords

organic nitrates; organic aerosol; urban air quality; aerosols; particulate matter; volatile organic compounds; nitrogen oxides; absorptive partitioning theory

1 Introduction

Organic aerosol (OA) constitutes a large, and often dominant, fraction of tropospheric aerosol mass[1-3]. Much of this organic aerosol is secondary (secondary organic aerosol, SOA), produced from volatile organic compounds (VOCs) that are sufficiently oxidized in the atmosphere to be condensable and/or water-soluble[4-8]. The chemical and physical processes that control SOA production, however, are complex and currently highly uncertain[1,9-16].

Particle phase organic nitrates ($pRONO_2$) have recently emerged as a significant component of SOA in areas dominated by biogenic emissions, including the Southeast US[17-22], in the Rocky Mountains[23], across Europe[24], in the boreal forest[25], in the California Central Valley[26,27], and in rural areas of both northern and southern China[28-30]. A number of studies have also found significant contributions of $pRONO_2$ to SOA in regions of oil

and gas production, including the Alberta Oil Sands[31] and in the Uintah Basin[32]. Recent observations have shown that organic nitrates are a significant contributor to OA in Chinese cities[33,34]. Specifically, Yu et al.[34] found that organic nitrates make up 9 – 25% of OA during spring - autumn in urban Shenzhen, and the dominant precursors to $pRONO_2$ included both biogenic (α-pinene, limonene, and camphene) and anthropogenic (styrene) VOCs.

Organic nitrates are produced from the oxidation of VOCs in the presence of NO_x(≡ NO + NO_2), as shown in Figure 1. During the daytime when photochemistry is active, OH oxidation of VOCs generates RO_2 radicals (R1). The minor product (branching ratio α) of the reaction of NO with RO_2 radicals are gas-phase organic nitrates ($gRONO_2$, R2). In the nocturnal residual layer away from fresh NO emissions, NO_3 radicals can add to the double bonds of alkenes to generate $gRONO_2$ (R3) e.g., [35].

$$RH + OH \longrightarrow RO_2 + H_2O \quad \text{(R1)}$$

$$RO_2 + NO \xrightarrow{\alpha} RONO_2 \quad \text{(R2)}$$

$$NO_3 + R_1 = R_2 \longrightarrow R_1(ONO_2) - R_2 \quad \text{(R3)}$$

If the $RONO_2$ generated from either the OH-initiated or NO_3-initiated reaction pathways have sufficiently low volatility, they may partition into the aerosol phase as particle-phase organic nitrates, $pRONO_2$ (Figure 1). At 273 K, the addition of a nitrate functional group reduces the saturation concentration of a given molecule by 2.23 orders of magnitude[36], thereby generating a lower volatility compound that may condense to form SOA.

In this study, we examine the contribution of $pRONO_2$ to OA in Seoul, Korea. As a megacity, Seoul has a complex mixture of urban emissions, including from a number of chemical facilities and from transport of emissions from China, that contribute to the aerosol burden[37,38], though[37] determined that the dominant precursors for SOA production in Seoul were locally emitted VOCs. To better understand the sources of SOA in Seoul, here we aim to quantify the contribution of $pRONO_2$ to the total OA mass and determine the precursors and processes that control the production of $pRONO_2$ in Korea using observations from the 2016 Korea-United States Air Quality (KORUS-AQ) measurement campaign.

2 Methods

Here, we introduce the KORUS-AQ campaign (Section 2.1), the TD-LIF measurements of $pRONO_2$ and (Section 2.2), the CU-AMS measurements of $pRONO_2$ and OA (Section 2.3), and our CMAQ simulations of $RONO_2$ over Northeast Asia during the time period of the KORUS-AQ campaign (Section 2.4).

2.1 KORUS-AQ

The KORUS-AQ campaign took place during May and June 2016 over the Korean peninsula and the Yellow Sea[39]. Seoul, Korea is bordered to the west by the Yellow Sea and Gyeonggi Bay and bordered to the north, east, and south by forested and mountainous regions[40]. During KORUS-AQ, winds were typically from the west or northwest, meaning that air over the Yellow Sea can be considered 'background' air for Seoul[41]. There are a number of large industrial facilities along the Northwest coast of South Korea, including the Daesan petrochemical complex which produces large amounts of VOC emissions[42].

This analysis uses observations from the NASA DC-8 which flew 20 research flights out of Pyeongtaek, South Korea (≈ 60 km south of Seoul). Flights typically began around 08:00 LT (KST). During a typical flight, three missed approaches were performed over the Seoul Air Base (within 15 km of Seoul city center): one soon after takeoff around 08:00 LT, one around 12:00 LT, and one prior to landing around 15:00 LT. Each missed approach included 15-45 minutes of observations within the boundary layer in the Seoul Metropolitan Area. Flights also consisted of transects west of Seoul over the Yellow Sea, south of Seoul to Jeju, and/or southeast of Seoul to Busan at varying altitudes, as shown in Figure 2. We use 60-second measurement averages in this analysis.

During KORUS-AQ, the NASA DC-8 was equipped with the only two currently aircraft certified techniques to measure total $pRONO_2$: the UC Berkeley thermal dissociation laser induced fluorescence (TD-LIF) instrument and the University of Colorado-Boulder high-resolution time-of-flight aerosol mass spectrometer (CU-AMS). Though some other measurement techniques exist to measure certain specific $RONO_2$ species [e.g., 43,44], the TD-LIF and CU-AMS measurement schemes allow for measurements of the sum of all $pRONO_2$ species.

2.2 TD-LIF measurements of $tRONO_2$ and $pRONO_2$

Measurements of $tRONO_2$ (gas + particle) were made using the UC TD-LIF instrument[45,46]. Briefly, one channel of the instrument measures NO_2 by laser induced fluorescence (LIF). Two other channels first flow air through a heated quartz oven. One channel is set at 180°C, the temperature at which peroxy nitrates (RO_2NO_2) dissociate into RO_2 and NO_2. The second is set at 360°C, the temperature at which $RONO_2$ dissociate into RO + NO_2. The difference in NO_2 detected in adjacent channels gives the mixing ratio for each class of compounds: the RO_2NO_2 mixing ratio corresponds to the difference between the 180°C channel and the unheated channel, and the $RONO_2$ mixing ratio corresponds to the difference between the 360°C channel and the 180°C channel.

$pRONO_2$ concentrations were measured using a fourth channel configured as described in Rollins et al. [47]. Before entering the heated section of the instrument, air passes through a 10 cm long activated carbon honeycomb denuder with an outer diameter of 2 cm which removes gas-phase compounds (MAST Carbon International Ltd. carbon monolith with 89 cells cm^{-2} where each open square is 0.63 by 0.63 mm with 0.43 mm thick walls in between). The particles that remain are then rapidly heated to vaporize the aerosols and dissociate the $RONO_2$ molecules present into RO and NO_2. NO_2 is then detected

via LIF, giving a measurement of $pRONO_2$. We estimate a limit of detection of 20 ppt of $pRONO_2$, or 0.055 $\mu g\ m^{-3}$ of NO_3. Though inorganic nitrate compounds will also be vaporized, volatile inorganic nitrate salts form HNO_3 when vaporized[48] and will therefore not interfere in this measurement. Empirical and theoretical studies confirm that NO_2, HNO_3, and gas-phase organic nitrates are all removed at nearly 100% efficiency in the charcoal denuder, while particles greater than 100 nm in diameter are transmitted with over 95% efficiency[47]. Recent work has shown that HONO is removed with near-100% efficiency in dry air and with 85% efficiency at an RH of 46% with a similar denuder[49]. Furthermore, during KORUS-AQ the denuder could be bypassed with a pair of 3-way valves, as shown in Figure S1. When bypassed, the NO_2 calibration mixture reached the $pRONO_2$ LIF cell. When not bypassed, the NO_2 calibration events served as checks for NO_2 breaking through the denuder. Compared to the 20 ppt limit stated above, no breakthroughs of the 12 or 24 ppb NO_2 calibration steps were detectable during the deployment as shown in Figure S6.

KORUS-AQ is the first time $pRONO_2$ measurements have been made with TD-LIF on aircraft. Previous ground-based measurements of $pRONO_2$ by the TD-LIF were made in the Rocky Mountains during BEACHON-RoMBAS[23], in the Uintah Basin[32], in the Southeast US during SOAS[21], and in the California Central Valley during CalNex[27].

We apply a small correction for the loss of charged particles to TD-LIF measurements of $tRONO_2$ and $pRONO_2$. In the TD-LIF inlet configuration during KORUS-AQ, air for all channels goes through 10 - 20 cm of PFA Teflon before heating. We performed a series of laboratory experiments (detailed in Section S1) to determine the loss of charged particles in these lengths of PFA Teflon tubing. Taking into account the ambient distribution of charged particles[50] and the observed aerosol size distribution during KORUS-AQ, there is less than 20% loss for charged particles with diameters less than 280 nm in the TD-LIF inlet.

We also apply a correction for inertial losses of particles in the TD-LIF inlet. We model the inertial losses on the two bends (90°and 98°) in the inlet (see Section S1) for varying particle sizes. We apply the size-dependent modeled losses to the aerosol volume distribution measured by laser aerosol spectrometer (LAS, Langley LARGE group). On average, we estimate that the TD-LIF observes ≈ 60% of the particles observed by LAS. We apply both particle loss corrections (charged and inertial) to both the $pRONO_2$ and $tRONO_2$ TD-LIF measurements.

2.3 CU-AMS measurements of $pRONO_2$

A second measurement of $pRONO_2$ was made by the CU-AMS (Aerodyne Research, Inc.). The CU-AMS also measured organic aerosol (OA) concentrations. A description of the CU-AMS aircraft sampling can be found in DeCarlo et al.[51], Canagaratna et al.[52], and Nault et al.[37].

The CU-AMS uses NO_x ion ratios (NO_2^+/NO^+) to differentiate between inorganic nitrate (NH_4NO_3) and organic nitrate ($pRONO_2$)[23,53], described further in Section S2. Uncertainties in this method are greatest when $pRONO_2$ < 20% of the total measured aerosol nitrate; those CU-AMS measurements have been removed from this analysis. This ion ratio technique has been used previously in rural environments where VOCs are dominantly

biogenic and $RONO_2$ concentrations are relatively small[17,23,54]. However, the high NH_4NO_3 loadings in the urban environment measured during KORUS-AQ create uncertainty for the CU-AMS measurement of $pRONO_2$.

Though we applied a series of corrections for particle loss in the TD-LIF inlet (described in Section 2.2), we could not entirely reconcile the differences between the two measurements. Since the two measurements may be prone to larger uncertainties under different aerosol size and composition conditions, we conduct the following analyses using both the TD-LIF and CU-AMS $pRONO_2$ measurements separately and treat them as upper and lower bounds. A comparison of the TD-LIF and CU-AMS measurements, both before and after corrections, can be seen in Figure S9.

Because the TD-LIF and CU-AMS $pRONO_2$ measurements do not agree perfectly, we also use a CU-AMS-adjusted $tRONO_2$ to ensure a consistent comparison. In the following calculations that use CU-AMS $pRONO_2$, we subtract the TD-LIF $pRONO_2$ measurement from the TD-LIF $tRONO_2$ measurement to give an estimate of the gas-phase $RONO_2$ measured by the TD-LIF ($gRONO_2$). We then add the CU-AMS $pRONO_2$ to the estimated TD-LIF $gRONO_2$ to generate the CU-AMS-adjusted $tRONO_2$.

2.4 CMAQ modeling of $RONO_2$ chemistry and phase partitioning

We ran the Community Multiscale Air Quality Modeling System (CMAQ) model v5.2[55,56] with the RACM2_Berkeley2.1 chemical mechanism[22,57] over Northeast Asia with a 15-km horizontal grid (17.4 - 47.2°N and 93.2-147.4°E) and 27 vertical layers. Meteorological fields were generated by WRF v3.8.1 and processed for use in CMAQ by MCIP v4.5[58]. The simulation period was April 17, 2016 - June 12, 2016, with the first 14 days as a spin-up period to minimize the impact of initial conditions.

We used the KORUSv5.0 anthropogenic emissions inventory developed at Konkuk University based on the CREATE emission inventory[59] which includes area, point, mobile, and ship emissions, MEGANv2.1 biogenic emissions[60], and FINNv1.5 fire emissions[61], all processed through the Sparse Matrix Operator Kernel Emissions (SMOKE) system[62]. The KORUSv5.0 emissions inventory was prepared using the SAPRC07T AERO6 mechanism, which we then converted to RACM2_Berkeley2.1 (detailed in Table S1).

We made a few adjustments to the emissions inventory informed by a series of comparisons between CMAQ modeled VOC concentrations and aircraft VOC measurements made with whole air samples (WAS) analyzed with multi-column gas chromatography[63]. We increased monoterpene emissions by a factor of three to improve the magnitude agreement between modeled and observed concentrations of monoterpenes (see Figure S12). Note we expect monoterpenes in Korea to have both biogenic as well as anthropogenic sources[64,65].

Comparison between modeled and observed BTEX (benzene, toluene, ethyl benzene, and xylenes) indicated that these species were also underestimated in the emissions inventory (see Figure S12). We updated BTEX emissions over the Daesan petrochemical complex to match emission fluxes calculated from observations using a mass balance approach by Fried et al.[42]. Elsewhere, we note that the spatial pattern of modeled TOL (defined as toluene

and less reactive aromatics, for measurement comparison purposes we approximate as the sum of toluene and ethyl benzene) corresponds well to the spatial pattern of the sum of measured toluene and ethyl benzene (see Figure S10). However, without any emissions corrections, the model underestimates boundary layer TOL by a factor of 1.4. We also note that measurements of other reactive aromatics (xylenes and 1,2,4-trimethyl benzene) correlate well with the sum of measured toluene and ethyl benzene (see Figure S11). As such, we scale TOL emissions by 1.4 and define the emissions of the other reactive aromatics based on their measured ratios to the sum of toluene and ethyl benzene. We use measured o-xylene as a proxy for model species XYO, the sum of measured m-xylene and 1,2,4-trimethyl benzene as a proxy for model species XYM, and measured p-xylene as a proxy for model species XYP. This method results in setting XYO emissions as 0.05× TOL, XYM emissions as 0.08× TOL, and XYP emissions as 0.07× TOL, such that XYO, XYM, and XYP emissions all follow the same spatial pattern as TOL.

We use the default initial conditions and boundary conditions from the initial condition (ICON) and boundary condition (BCON) processors in CMAQ v5.2. However, measurements of isoprene-derived nitrates by Caltech's Chemical Ionization Mass Spectrometer (CIT-CIMS)[66] indicated that longer-lived propanone nitrate and ethanal nitrate were underestimated in CMAQ. Consequently, we increased the boundary and initial condition concentrations of propanone nitrate and ethanal nitrate to match the CIT-CIMS observations of both nitrates over the Yellow Sea (propanone nitrate = 21.5 ppt; ethanal nitrate = 4.1 ppt).

The original RACM2 (Regional Atmospheric Chemistry Mechanism) mechanism[67] is available in CMAQ v5.0.2 and later versions[68]. Browne et al.[69] modified the mechanism to RACM2_Berkeley to expand the organic nitrate chemistry. New species, along with their corresponding oxidation rates and branching ratios, were added to further classify anthropogenic nitrates[70-72] and to represent monoterpene nitrates[73-76]. The parameterization of OH-initiated isoprene oxidation was also updated[77-79]. RACM2_Berkeley was evaluated using aircraft observations over the Canadian boreal forest[69].

RACM2_Berkeley was updated to RACM2_Berkeley2 in Zare et al.[57] to reflect recent advances in the representation of OH- and NO_3- initiated BVOC oxidation under both low- and high-NO_x conditions, with a focus on a detailed representation of nitrates derived from NO_3-initiated oxidation of isoprene and on the fate of the most important individual biogenically-derived organic nitrates. Deposition rates were also updated.

Zare et al.[22] revised RACM2_Berkeley2 to RACM2_Berkeley2.1 to include an explicit representation of multi-phase organic nitrate formation and loss, including vapor-pressure driven partitioning into organic aerosol, aqueous-phase uptake, and condensed-phase reactions. Further updates were also done to explicitly represent isoprene nitrates from NO_3 oxidation that are subject to reactive uptake to the aerosol phase. As such, the RACM2_Berkeley2.1 mechanism represents our current understanding of $RONO_2$ chemistry and phase partitioning. Zare et al.[22] evaluated this mechanism (implemented in CMAQ) using observations from the Southern Oxidant and Aerosol Study (SOAS) campaign in the Southeast US during summer 2013. Inclusion of the particle-phase pathways for $RONO_2$

improved the model-measurement agreement for $tRONO_2$, and the modeled fraction of $tRONO_2$ in the particle phase (F_p) was within the range of observed F_p.

To compare modeled and measured concentrations, we sample CMAQ coincidentally in time (hourly resolution) and horizontal space with each observation. All comparisons in the following analysis use boundary layer measurements (< 1, 000 m) and the average of the bottom three model layers.

3 Results

Maps of average TD-LIF measured and CMAQ modeled $tRONO_2$ used in the following analysis are shown in Figure 2. Both the measurements and model indicate that $tRONO_2$ concentrations are highest in and around Seoul. However, the model consistently underpredicts $tRONO_2$ concentrations throughout the region. For reference, CMAQ predicts that > 95% of $pRONO_2$ are derived from vapor-pressure dependent partitioning into organic aerosol, whereas < 5% of $pRONO_2$ enter the particle phase through aqueous pathways, similar to what Zare et al.[22] found for the Southeast US.

3.1 $RONO_2$ partition into the aerosol phase and can be a significant contribution to SOA

We explore the average phase partitioning behavior of $RONO_2$ during KORUS-AQ in Figure 3. Our observations from both the TD-LIF and CU-AMS indicate that, on average, 1/4 of $tRONO_2$ is in the condensed phase and therefore contributes to the OA burden. We also consider a line, drawn above most measurement means, that represents a reasonable upper limit of 35% for the fraction of $tRONO_2$ in the particle phase.

To quantify the contribution of $pRONO_2$ to total OA concentrations, we assume an average molecular weight for $pRONO_2$ of 300 g mol^{-1}[27]. We expect condensable $RONO_2$ to be highly oxidized, contain at least one nitrate group (molecular weight = 62 g mol^{-1}) and to therefore have relatively high masses. With this assumption, we estimate that ≈ 15% of the OA mass can be attributed to $pRONO_2$, as shown in Figure 3. Note that this estimate does not include CU-AMS measurements when $pRONO_2$ ¡ 20% of total measured aerosol nitrate. We again consider a reasonable upper limit, drawn above most measurement means, to estimate that a maximum of 40% of OA can be attributed to $pRONO_2$. This is within the range of $pRONO_2$ contributions to OA mass measured across Europe (42%)[24], in a suite of studies across the eastern US, western US and Europe (5-73%)[80], and in recent studies in urban and rural China (9-28%)[34,81].

3.2 Observations indicate $RONO_2$ phase partitioning is controlled by absorptive partitioning into OA

Previous studies have shown that vapor pressure controls the phase of organic nitrates[22,27]. This equilibrium absorptive partitioning follows Raoult's Law: the fraction of $RONO_2$ in the particle phase increases with increasing mass of the absorbing or solvating aerosol, namely total organic aerosol[82,83]. Accordingly, the equilibrium fraction of an individual $RONO_2$ species i in the particle phase ($F_{p,i}$) is given by

$$F_{p,i} = \frac{C_{p,i}}{C_i} = \frac{C_{OA} / C_i^*(T)}{1 + C_{OA} / C_i^*(T)} = \left(1 + \frac{C_i^*(T)}{C_{OA}}\right)^{-1} \quad (1)$$

Here, $C_{p,i}$ and C_i are the particle phase and total concentrations of species i, respectively. $C_i^*(T)$ is the temperature-dependent saturation concentration (μg m^{-3}) of species i, and C_{OA} is the concentration of total OA.

For both the TD-LIF and CU-AMS measurements of pRONO$_2$, the fraction of RONO$_2$ in the particle phase (F_p) increases with increasing OA concentration and increases with decreasing temperature, as shown in Figure 4. Assuming the speciation of RONO$_2$ is invariant with temperature, these relationships between F_p, OA, and temperature indicate that the phase partitioning of RONO$_2$ during KORUS-AQ is indeed controlled by equilibrium absorptive partitioning.

To determine the volatility distribution of RONO$_2$ observed during KORUS-AQ, we define a saturation concentration basis set of $\{C_j^*\} = \{3, 30, 300\}$, μg m^{-3}, mfollowing the convention of Donahue et al.[82]. Though we expect some RONO$_2$ species to have volatilities outside of this range, because the OA concentrations we observe during KORUS-AQ do not exceed 40 μg m^{-3} we cannot reasonably constrain volatilities outside of this defined basis set. Given this basis set, the total fraction of organic nitrates in the particle phase ($F_{p,tot}$) can be represented as

$$F_{p,tot} = \frac{\Sigma_i C_i F_{p,i}}{\Sigma_i C_i} = \sum_{j=1}^{n} f_j \left(1 + \frac{C_j^*}{C_{OA}}\right)^{-1} \quad (2)$$

Here, f_j is the fraction of organic nitrates that can be classified as having saturation concentration C_j^*, and $n = 3$ for the basis set defined earlier.

We solve for each f_j in Equation 2 using our observations of $F_{p,tot}$ (= pRONO$_2$ / RONO$_2$) and organic aerosol concentrations (C_{OA}). Moreover, because saturation concentration is dependent on temperature, we separate the observations into a series of temperature bins and solve for fitting parameters f_j in each temperature bin, as shown in Figure 4 for both TD-LIF and CU-AMS observations. As expected, organic nitrates become less volatile at lower temperatures. At all temperatures, 10-39% of organic nitrates can be represented with $C^* \leq 3$ μg m^{-3}, meaning they will dominantly be condensed at the average observed organic aerosol concentrations of ≈ 9.8 μg m^{-3}. At high temperatures (≈ 300 K), 73-76% of organic nitrates can be represented with $C^* \geq 300$ μg m^{-3}, meaning that they will dominantly remain in the gas phase at observed OA concentrations. At low temperatures (≈ 286 K), the TD-LIF measurements suggest that 67% of organic nitrates can be represented with $C^* \geq 300$ μg m^{-3} and the CU-AMS measurements suggest 61% of organic nitrates can be represented with $C^* \geq 30$ μg m^{-3}.

We also fit the data to Equation 2 using an empirical relationship between C^* and ΔH_{vap} from Epstein et al.[84] to examine the variation of $RONO_2$ volatilities observed at different temperatures but referenced to 300 K. Figure S15 shows the distribution of C^*(300 K) for $RONO_2$ during KORUS-AQ.

3.3 CMAQ modeling misses a large source of semivolatile, anthropogenically-derived $RONO_2$

To test the efficacy of our simulations, we compare modeled and measured NO_x, O_3, and O_x($\equiv O_3 + NO_2$) mixing ratios at the Olympic Park ground site in Seoul, as shown in Figure S13. Our CMAQ simulation is able to capture the diurnal patterns in NO_x, O_3, and O_x and does not show a systematic under- or over-estimation. Additionally, we compare measured and modeled OA concentrations at KIST (Korea Institute of Science and Technology, Seoul) during the campaign (see Figure S13). The CMAQ simulation is able to accurately capture the regional OA background concentration and many of the episodic events with elevated OA. Moreover, a multi-model inter-comparison study of air quality simulations for the KORUS-AQ campaign used comparisons of PM_1 to show that models, including CMAQ, were generally able to capture the synoptic meteorological patterns during the campaign[85]. We also include a comparison of measured and modeled temperature on the DC-8 in Figure S13 which shows that our CMAQ simulations are able to capture the observed variability in temperature.

However, our CMAQ simulation underpredicts measured $tRONO_2$ concentrations by a factor of ≈ 3, as shown by the slopes reported in Table 1 and plotted in Figure S14. Moreover, our CMAQ simulation underpredicts measured $pRONO_2$ concentrations by a factor of ≈ 10, indicating that the $RONO_2$ in CMAQ are too volatile. These underpredictions for both $tRONO_2$ and $pRONO_2$ indicate that our simulation is missing a large source of condensable $RONO_2$. We note that the RACM2_Berkeley2.1 mechanism does not include Cl-initiated oxidation of VOCs; however, based on observations, we estimate that the production rate of RO_2 radicals from Cl oxidation is an order of magnitude slower than that from OH-initiated oxidation (see Section S6) and is therefore insufficient to explain the missing source of $RONO_2$.

To help determine the origin of the missing source of $RONO_2$, we examine the correlation between the model-measurement $RONO_2$ difference ($RONO_{2,diff}$) and measurements of various VOC classes. We find $R^2 < 0.05$ for the correlation between $RONO_{2,diff}$ and both isoprene and α-pinene, whereas there are relatively stronger correlations between $RONO_{2,diff}$ and anthropogenic alkanes ($R^2 = 0.15$), alkenes ($R^2 = 0.12$), aromatics ($R^2 = 0.23$), and aldehydes ($R^2 = 0.67$). The weak correlations between the $RONO_{2,diff}$ and VOCs of biogenic origin and the relatively stronger correlations between $RONO_{2,diff}$ and VOCs of anthropogenic origin suggest that the missing source of condensable $RONO_2$ is derived from anthropogenic VOCs.

Note that the missing source of $RONO_2$ over the Korean peninsula is likely derived from both transport of $RONO_2$ produced in China as well as from locally-produced $RONO_2$. As shown in Figure 2, CMAQ underpredicts $RONO_2$ over the Yellow Sea, a region influenced by transport of air from China during parts of the KORUS-AQ campaign, as well as over

the urban centers of the Korean peninsula where local chemistry contributes to the observed $RONO_2$.

Furthermore, the RACM2_Berkeley2.1 mechanism was initially tested and validated on a regional scale over the Southeast US, an area dominated by biogenic emissions[22,57]. Additionally, as described in Section 2.4, we adjusted the emissions of monoterpenes to improve the model-measurement agreement for biogenic VOCs. Though we expect some change in the oxidation product distribution between low-NO_x environments (e.g., Southeast US) and high-NO_x environments (e.g., Seoul), we are reasonably confident that our CMAQ simulation is accurately capturing the production and fate of $RONO_2$ derived from biogenic VOCs. We therefore attribute the missing source of $RONO_2$ in our simulations to $RONO_2$ of anthropogenic origin. This previous work evaluating RACM2_Berkeley2.1 in the Southeast US[22,57] did not look at urban $RONO_2$ in the US, but we have no reason to suspect that this missing source of condensable $RONO_2$ is not a general phenomenon.

The relationship between CMAQ-modeled $F_p(RONO_2)$, OA, and temperature is shown in Figure 4c. In contrast to the observations (Figure 4a,b) and in contrast with absorptive partitioning theory, the modeled F_p increases with increasing temperature and decreases with increasing OA. Exploration of the speciated distribution of modeled $RONO_2$ (shown in Figure S16) indicates that the increase in modeled F_p with temperature is driven largely by a temperature-dependent change in the $RONO_2$ speciation. The phase partitioning of each $RONO_2$ species is controlled by absorptive partitioning, meaning the fraction of an individual $RONO_2$ species in the particle phase increases with decreasing temperature. However, the modeled increase in the total concentration of low-volatility monoterpene nitrates (HONIT) with temperature is larger than the modeled change in concentration of other higher-volatility nitrates with temperature. As a result, the concentration of $pRONO_2$ increases with increasing temperature faster than the concentration of $gRONO_2$ increases with temperature, causing the total F_p to increase with increasing temperature. This modeled relationship between F_p and temperature stands in stark disagreement with the observations and therefore indicates that the species distribution of $RONO_2$ over Korea is incorrectly captured in our CMAQ simulation.

To test and quantify our hypothesis that our CMAQ simulation is missing a large source of condensable, anthropogenic $RONO_2$, we test the effect of adding an additional source of $RONO_2$. Because our CMAQ simulation underpredicts measured $tRONO_2$ concentrations by a factor of ≈ 3 (Table 1), we assign this additional source to have double the concentration of the existing simulated $RONO_2$. To determine the average volatility of this missing source of $RONO_2$, we iteratively vary its assigned C^* by order of magnitude (e.g., C^* = 30, 300, 3000 $\mu g\ m^{-3}$) and use an empirical relationship between C^* and ΔH_{vap} from Epstein et al.[84]. We find the best agreement between modeled and measured $pRONO_2$ and F_p with C^* = 300 $\mu g\ m^{-3}$ as shown in Table S2. Though comparison between modeled and measured $RONO_2$ remains relatively scattered (see Figure S14) and the missing source likely includes a variety of molecules with a range of volatilities, adding this missing semivolatile $RONO_2$ source improves the magnitude of the model-measurement agreement for $tRONO_2$, $pRONO_2$, and F_p, as shown in Table 1. Moreover, as shown in Figure 4, addition of this unknown source of relatively condensable $RONO_2$ results in an increase in F_p with decreasing temperature

and increasing OA concentration. This relationship between F_p, temperature, and OA is in agreement with the observations and with equilibrium absorptive partitioning theory.

4 Discussion

The RACM2_Berkeley2.1 mechanism represents our state-of-the-science understanding of $RONO_2$ chemistry, where the only sources of semi-volatile $RONO_2$ are biogenic. However, this mechanism only captures one third of the $RONO_2$ production over the Korean peninsula. Moreover, the unknown source of organic nitrates consists of $RONO_2$ that are lower volatility than most of the existing $RONO_2$ in the model. Consequently, our current understanding of $RONO_2$ chemistry is missing pathways for semivolatile $RONO_2$ production as a result of either missing oxidation pathways (first- or multi-generation, bimolecular or unimolecular) or an underestimation of $RONO_2$ yields.

Because the known chemistry can only account for one third of the observed $RONO_2$, the missing source is approximately double in magnitude to the known sources. During KORUS-AQ, the average reactivity of all measured VOCs with OH was 2.4 s^{-1}, and the effective average $RONO_2$ yield (α), weighted by reactivity, was 1.3%. If the unknown source of $RONO_2$ has a low α of 1%, the missing reactivity must be ≈ 3 s^{-1}. On the other hand, if the unknown source of $RONO_2$ has a higher α of 20%, the missing reactivity must be ≈ 0.15 s^{-1}. For reference, during KORUS-AQ the average isoprene reactivity was 0.051 s^{-1} and the average toluene reactivity was 0.054 s^{-1}.

We hypothesize three potential missing sources of semivolatile $RONO_2$: (1) missing source(s) of semi- and intermediate-volatility organic compounds (S/IVOCs) that are oxidized to $RONO_2$; (2) unrepresented autoxidation mechanisms that produce highly oxygenated organic peroxy radicals (RO_2) which could react with NO to form $RONO_2$; or (3) more generations of bimolecular oxidation than are currently represented.

S/IVOCs are considered major SOA precursors [e.g., 12,14,37,86-93], but their concentrations are challenging to measure in the atmosphere due to condensation within instruments [e.g., 94], and their chemistry is difficult to measure in chamber experiments due to wall loss [e.g., 95]. Nault et al.[37] concluded that, during KORUS-AQ, S/IVOCs and reactive aromatics contributed to 70% of the total SOA over Seoul. Because they are emitted with relatively low volatility, oxidation of S/IVOCs to form $RONO_2$ could contribute to the missing source of semivolatile $RONO_2$. Because the addition of a nitrate group decreases a molecule's volatility by ≈ 2.2 orders of magnitude[36], a missing $RONO_2$ source with saturation concentration 300 $\mu g\ m^{-3}$ implies a precursor with $C^* = 10^5\ \mu g\ m^{-3}$, namely an IVOC. The contribution of S/IVOCs to $pRONO_2$ is not unprecedented; Lee et al.[31] determined that much of the $pRONO_2$ formation in the Alberta oil sands occurred via photo-oxidation of IVOCs under high-NO_x conditions.

Autoxidation, a mechanism involving an intramolecular hydrogen-shift followed by addition of molecular oxygen in RO_2 radicals, can quickly (in seconds) generate highly oxygenated molecules, or HOMs[96,97] and references therein. Because of their high oxygen content, HOMs have significantly reduced volatility compared to their parent VOCs [e.g., 98-100]. Although autoxidation becomes relatively more competitive with bimolecular oxidation

pathways as NO_x decreases, absolute rates of autoxidation increase with increasing NO_x due to increased oxidant availability[101]. In Korea's high-NO_x environment, autoxidation may generate highly oxidized RO_2 which could produce $RONO_2$ via reaction with NO (R2). While most previous studies of HOMs have focused on autoxidation of RO_2 derived from biogenic VOCs, theoretical calculations by Wang et al.[102] indicate that substituted benzenes, which were measured in high abundance during KORUS-AQ[42,63], may also produce HOMs through autoxidation of bicyclic peroxy radicals. Beginning with a substituted benzene molecule with $C^* \approx 10^7$ $\mu g\ m^{-3}$, one hydrogen-shift reaction resulting in the addition of a hydroperoxide group would reduce the volatility by ≈ 2.5 orders of magnitude, and further addition of a nitrate group would reduce the volatility by ≈ 2.2 orders of magnitude[36], resulting in a $C^* \approx 10^2$ $\mu g\ m^{-3}$ compound. Consequently, only one hydrogen-shift reaction is necessary to convert a substituted aromatic compound to a nitrate of the missing volatility.

Additionally, multiple recent studies have suggested that multi-generation OH oxidation of aromatics can lead to highly oxygenated oxidation products, many of which, particularly under high-NO_x conditions, contain nitrogen [e.g., 103-105]. Some of these nitrogen-containing products are likely organic nitrates, but the nitrogen-containing product distribution also includes peroxy nitrates and nitro aromatics. Because aromatics are a large contributor to total VOCs over Korea[42,63], there could be significant production of semivolatile, multi-functional, oxygenated organic nitrates from multi-generation oxidation of aromatic VOCs.

In summary, exploration of the phase partitioning of $RONO_2$ over the Korean peninsula using our aircraft-based measurements of $pRONO_2$ and $tRONO_2$ during KORUS-AQ, as an example of urban chemistry, indicate that organic nitrates contribute ≈ 15% of the total OA. This significant contribution of organic nitrates to the OA burden, as has been observed elsewhere, reinforces the notion that a better understanding of the processes that control the production, loss, and phase partitioning of $RONO_2$ are crucial for understanding the processes that control SOA production and loss. Our current understanding of $RONO_2$ chemistry can only explain one third of the observed $RONO_2$ in Korea and is therefore missing a source of semi-volatile, anthropogenically-derived $RONO_2$ in and around Seoul. We recommend further laboratory and field research to determine the source VOCs and mechanisms that drive the production of this missing source of organic nitrates.

Supplementary Material

Refer to Web version on PubMed Central for supplementary material.

Acknowledgement

This work was supported by NASA grant 80NSSC18K0624 and an NSF GRFP for HSK (DGE1106400). BAN, PCJ, DAD, and JLJ acknowledge NASA grant NNX15AT96G and 80NSSC18K0630 for support. This research used the Savio computational cluster resource provided by the Berkeley Research Computing program at the University of California, Berkeley (supported by the UC Berkeley Chancellor, Vice Chancellor of Research, and Office of the CIO). We thank the Wennberg group at Caltech for use of their second generation isoprene nitrate measurements and the NASA Langley LARGE team for their LAS measurements.

KORUS-AQ data are available at http://doi.org/10.5067/Suborbital/KORUSAQ/DATA01. CMAQ model code associated with this work can be found in the Environmental Protection Agency Science Hub repository (https://catalog.data.gov/harvest/about/epa-sciencehub, DOI: 10.23719/1503432). RACM2_Berkeley2.1 mechanism code can be found at https://github.com/CohenBerkeleyLab/MECH_RACM.

The US Environmental Protection Agency, through its Office of Research and Development, collaborated in the research described here. The research has been subjected to Agency administrative review and approved for publication but may not necessarily reflect official Agency policy. The views expressed in this Article are those of the authors and do not necessarily represent the views or policies of the US Environmental Protection Agency.

References

(1). Heald CL; Jacob DJ; Park RJ; Russell LM; Huebert BJ; Seinfeld JH; Liao H; Weber RJ A large organic aerosol source in the free troposphere missing from current models. Geophysical Research Letters 2005, 32, 1–4.

(2). Murphy DM; Cziczo DJ; Froyd KD; Hudson PK; Matthew BM; Middlebrook AM; Peltier RE; Sullivan A; Thomson DS; Weber RJ Single-particle mass spectrometry of tropospheric aerosol particles. Journal of Geophysical Research 2006, 111, 1–15. [PubMed: 20411040]

(3). Zhang Q; Jimenez JL; Canagaratna MR; Allan JD; Coe H; Ulbrich I; Alfarra MR; Takami A; Middlebrook AM; Sun YL; Dzepina K; Dunlea E; Docherty K; Decarlo PF; Salcedo D; Onasch T; Jayne JT; Miyoshi T; Shimono A; Hatakeyama S; Takegawa N; Kondo Y; Schneider J; Drewnick F; Cottrell L; Griffin RJ; Rautiainen J; Sun JY; Zhang YM Ubiquity and dominance of oxygenated species in organic aerosols in anthropogenically-influenced Northern Hemisphere midlatitudes. Geophysical Research Letters 2007, 34, 1–6.

(4). de Gouw JA; Middlebrook AM; Warneke C; Goldan PD; Kuster WC; Roberts JM; Fehsenfeld FC; Worsnop DR; Canagaratna MR; Pszenny AAP; Keene WC; Marchewka M; Bertman SB; Bates TS Budget of organic carbon in a polluted atmosphere : Results from the New England Air Quality Study in 2002. Journal of Geophysical Research 2005, 110, 1–22.

(5). de Gouw JA; Brock CA; Atlas EL; Bates TS; Fehsenfeld FC; Goldan PD; Holloway JS; Kuster WC; Lerner BM; Matthew BM; Middlebrook AM; Onasch TB; Peltier RE; Quinn PK; Senff CJ; Stohl A; Sullivan AP; Trainer M; Warneke C; Weber RJ; Williams EJ Sources of particulate matter in the northeastern United States in summer: 1 . Direct emissions and secondary formation of organic matter in urban plumes. Journal of Geophysical Research 2008, 113, 1–19.

(6). Goldstein AH; Galbally IE Known and Unexplored Organic Constituents in the Earth's Atmosphere. Environmental Science & Technology 2007, 1515–1521.

(7). Jimenez JL; Canagaratna MR; Donahue NM; Prevot ASH; Zhang Q; Kroll JH; Decarlo PF; Allan JD; Coe H; Ng NL; Aiken AC; Ulbrich IM; Grieshop AP; Duplissy J; Wilson KR; Lanz VA; Hueglin C; Sun YL; Tian J; Laaksonen A; Raatikainen T; Rautiainen J; Vaattovaara P; Ehn M; Kulmala M; Tomlinson JM; Cubison MJ; Dunlea EJ; Alfarra MR; Williams PI; Bower K; Kondo Y; Schneider J; Drewnick F; Borrmann S; Weimer S; Demerjian K; Salcedo D; Cottrell L; Takami A; Miyoshi T; Shimono A; Sun JY; Zhang YM; Dzepina K; Sueper D; Jayne JT; Herndon SC; Williams LR; Wood EC; Middlebrook AM; Kolb CE; Baltensperger U; Worsnop DR Evolution of Organic Aerosols in the Atmosphere. Science 2009, 326, 1525–1530. [PubMed: 20007897]

(8). Hodzic A; Campuzano-Jost P; Bian H; Chin M; Colarco PR; Day DA; Froyd KD; Heinold B; Jo DS; Katich JM; Kodros JK; Nault BA; Pierce JR; Ray E; Schacht J; Schill GP; Schroder JC; Schwarz JP; Sueper DT; Tegen I; Tilmes S; Tsigaridis K; Yu P; Jimenez JL Characterization of organic aerosol across the global remote troposphere: A comparison of ATom measurements and global chemistry models. Atmospheric Chemistry and Physics 2020, 20, 4607–4635.

(9). Volkamer R; Jimenez JL; Martini FS; Dzepina K; Zhang Q; Salcedo D; Molina LT; Worsnop DR; Molina MJ Secondary organic aerosol formation from anthropogenic air pollution : Rapid and higher than expected. Geophysical Research Letters 2006, 33, 1–4.

(10). Hallquist M; Wenger JC; Baltensperger U; Rudich Y; Simpson D; Claeys M; Dommen J The formation , properties and impact of secondary organic aerosol : current and emerging issues. Atmospheric Chemistry and Physics 2009, 9, 5155–5236.

(11). Heald CL; Kroll JH; Jimenez JL; Docherty KS; Decarlo PF; Aiken AC; Chen Q; Martin ST; Farmer DK; Artaxo P A simplified description of the evolution of organic aerosol composition in the atmosphere. Geophysical Research Letters 2010, 37, 1–5.

(12). Hayes PL; Carlton AG; Baker KR; Ahmadov R; Washenfelder RA; Alvarez S; Rappenglück B Modeling the formation and aging of secondary organic aerosols in Los Angeles during CalNex 2010. Atmospheric Chemistry and Physics 2015, 15, 5773–5801.

(13). Woody MC; Baker KR; Hayes PL; Jimenez JL; Koo B; Pye HOT Understanding sources of organic aerosol during CalNex-2010 using the CMAQ-VBS. Atmospheric Chemistry and Physics 2016, 16, 4081–4100.

(14). Ma PK; Zhao Y; Robinson AL; Worton DR; Goldstein AH; Ortega AM Evaluating the impact of new observational constraints on P-S/IVOC emissions, multi-generation oxidation, and chamber wall losses on SOA modeling for Los Angeles, CA. Atmospheric Chemistry and Physics 2017, 17, 9237–9259.

(15). Shrivastava M; Cappa CD; Fan J; Goldstein AH; Guenther AB; Jimenez JL; Kuang C; Laskin A; Martin ST; Ng NL; Petaja T; Pierce JR; Rasch PJ; Roldin P; Seinfeld JH; Shilling J; Smith JN; Thornton JA; Volkamer R; Wang J; Worsnop DR; Zaveri RA; Zelenyuk A; Zhang Q Recent advances in understanding secondary organic aerosol: Implications for global climate forcing. Reviews of Geophysics 2017, 55, 509–559.

(16). Tsimpidi AP; Karydis VA; Pandis SN; Lelieveld J Global-scale combustion sources of organic aerosols : sensitivity to formation and removal mechanisms. Atmospheric Chemistry and Physics 2017, 17, 7345–7364.

(17). Ayres BR; Allen HM; Draper DC; Brown SS; Wild RJ; Jimenez JL; Day DA; Campuzano-Jost P; Hu W; De Gouw J; Koss A; Cohen RC; Duffey KC; Romer P; Baumann K; Edgerton ES; Takahama S; Thornton JA; Lee BH; Lopez-Hilfiker FD; Mohr C; Wennberg PO; Nguyen TB; Teng A; Goldstein AH; Olson K; Fry JL Organic nitrate aerosol formation via NO3 + biogenic volatile organic compounds in the southeastern United States. Atmospheric Chemistry and Physics 2015, 15, 13377–13392.

(18). Pye HO; Luecken DJ; Xu L; Boyd CM; Ng NL; Baker KR; Ayres BR; Bash JO; Baumann K; Carter WP; Edgerton E; Fry JL; Hutzell WT; Schwede DB; Shepson PB Modeling the Current and Future Roles of Particulate Organic Nitrates in the Southeastern United States. Environmental Science and Technology 2015, 49, 14195–14203. [PubMed: 26544021]

(19). Xu L; Guo H; Boyd CM; Klein M; Bougiatioti A; Cerully KM; Hite JR; Isaacman-VanWertz G; Kreisberg NM; Knote C; Olson K; Koss A; Goldstein AH; Hering SV; De Gouw J; Baumann K; Lee SH; Nenes A; Weber RJ; Ng NL Effects of anthropogenic emissions on aerosol formation from isoprene and monoterpenes in the southeastern United States. Proceedings of the National Academy of Sciences of the United States of America 2015, 112, 37–42. [PubMed: 25535345]

(20). Fisher JA; Jacob DJ; Travis KR; Kim PS; Marais EA; Chan C; Yu K; Zhu L; Yantosca RM; Sulprizio MP; Mao J; Wennberg PO; Crounse JD; Teng AP; Nguyen TB; Clair JMS; Cohen RC; Romer P; Nault BA; Wooldridge PJ; Jimenez JL; Campuzano-jost P; Day DA Organic nitrate chemistry and its implications for nitrogen budgets in an isoprene- and monoterpenerich atmosphere : constraints from aircraft (SEAC^{4}RS) and ground-based (SOAS) observations in the Southeast US. Atmospheric Chemistry and Physics 2016, 16, 5969–5991. [PubMed: 29681921]

(21). Lee BH; Mohr C; Lopez-Hilfiker FD; Lutz A; Hallquist M; Lee L; Romer P; Cohen RC; Iyer S; Kurtén T; Hu W; Day DA; Campuzano-Jost P; Jimenez JL; Xu L; Ng NL; Guo H; Weber RJ; Wild RJ; Brown SS; Koss A; de Gouw J; Olson K; Goldstein AH; Seco R; Kim S; McAvey K; Shepson PB; Starn T; Baumann K; Edgerton ES; Liu J; Shilling JE; Miller DO; Brune WH; Schobesberger S; D'Ambro EL; Thornton JA Highly functionalized organic nitrates in the southeast United States: Contribution to secondary organic aerosol and reactive nitrogen budgets. Proceedings of the National Academy of Sciences 2016, 113, 1516–1521.

(22). Zare A; Fahey KM; Sarwar G; Cohen RC; Pye HOT Vapor-Pressure Pathways Initiate but Hydrolysis Products Dominate the Aerosol Estimated from Organic Nitrates. ACS Earth and Space Chemistry 2019, 3, 1426–1437. [PubMed: 31667449]

(23). Fry JL; Draper DC; Zarzana KJ; Campuzano-Jost P; Day DA; Jimenez JL; Brown SS; Cohen RC; Kaser L; Hansel A; Cappellin L; Karl T; Hodzic Roux A; Turnipseed A; Cantrell C; Lefer BL; Grossberg N Observations of gas- and aerosol-phase organic nitrates at BEACHON-RoMBAS 2011. Atmospheric Chemistry and Physics 2013, 13, 8585–8605.

(24). Kiendler-Scharr A; Mensah AA; Friese E; Topping D; Nemitz E; Prevot AS; Äijälä M; Allan J; Canonaco F; Canagaratna M; Carbone S; Crippa M; Dall Osto M; Day DA; De Carlo P; Di Marco CF; Elbern H; Eriksson A; Freney E; Hao L; Herrmann H; Hildebrandt L; Hillamo R; Jimenez JL; Laaksonen A; McFiggans G; Mohr C; O'Dowd C; Otjes R; Ovadnevaite J; Pandis

SN; Poulain L; Schlag P; Sellegri K; Swietlicki E; Tiitta P; Vermeulen A; Wahner A; Worsnop D; Wu HC Ubiquity of organic nitrates from nighttime chemistry in the European submicron aerosol. Geophysical Research Letters 2016, 43, 7735–7744.

(25). Hao LQ; Kortelainen A; Romakkaniemi S; Portin H; Jaatinen A; Leskinen A; Komppula M; Miettinen P; Sueper D; Pajunoja A; Smith JN; Lehtinen KE; Worsnop DR; Laaksonen A; Virtanen A Atmospheric submicron aerosol composition and particulate organic nitrate formation in a boreal forestland-urban mixed region. Atmospheric Chemistry and Physics 2014, 14, 13483–13495.

(26). Rollins AW; Browne EC; Min K-E; Pusede SE; Wooldridge PJ; Gentner DR; Goldstein AH; Liu S; Day DA; Russell LM; Cohen RC Evidence for NOx Control over Nighttime SOA Formation. Science 2012, 337, 1210–1212. [PubMed: 22955831]

(27). Rollins AW; Pusede S; Wooldridge P; Min KE; Gentner DR; Goldstein AH; Liu S; Day DA; Russell LM; Rubitschun CL; Surratt JD; Cohen RC Gas/particle partitioning of total alkyl nitrates observed with TD-LIF in Bakersfield. Journal of Geophysical Research Atmospheres 2013, 118, 6651–6662.

(28). Zhu Q; He LY; Huang XF; Cao LM; Gong ZH; Wang C; Zhuang X; Hu M Atmospheric aerosol compositions and sources at two national background sites in northern and southern China. Atmospheric Chemistry and Physics 2016, 16, 10283–10297.

(29). Xu W; Takeuchi M; Chen C; Qiu Y; Xie C; Xu W; Ma N; Worsnop D; Ng NL; Sun Y Estimation of particulate organic nitrates from thermodenuder-aerosol mass spectrometer measurements in North China Plain. Atmospheric Measurement Techniques Discussions 2020, 1–20.

(30). Zhu Q; Cao L-M; Tang M-X; Huang X-F; Saikawa E; He L-Y Characterization of Organic Aerosol at a Rural Site in the North China Plain Region: Sources, Volatility and Organonitrates. Advances in Atmospheric Sciences 2021, 38, 1115–1127.

(31). Lee AKY; Adam MG; Liggio J; Li S-M; Li K; Willis MD; Abbatt JPD; Tokarek TW; Odame-Ankrah CA; Osthoff HD; Strawbridge K; Brook JR A Large Contribution of Anthropogenic Organo-Nitrates to Secondary Organic Aerosol in the Alberta Oil Sands. Atmospheric Chemistry and Physics 2019, 19, 12209–12219.

(32). Lee L; Wooldridge PJ; DeGouw JA; Brown SS; Bates TS; Quinn PK; Cohen RC Particulate organic nitrates observed in an oil and natural gas production region during wintertime. Atmos. Chem. Phys 2015, 15, 9313–9325.

(33). Zhang JK; Cheng MT; Ji DS; Liu ZR; Hu B; Sun Y; Wang YS Characterization of submicron particles during biomass burning and coal combustion periods in Beijing, China. Science of the Total Environment 2016, 562, 812–821.

(34). Yu K; Zhu Q; Du K; Huan XF Characterization of nighttime formation of particulate organic nitrates based on high-resolution aerosol mass spectrometry in an urban atmosphere in China. Atmospheric Chemistry and Physics 2019, 19, 5235–5249.

(35). Fry JL; Brown SS; Middlebrook AM; Edwards PM; Campuzano-Jost P; Day DA; Jimenez JL; Allen HM; Ryerson TB; Pollack I; Graus M; Warneke C; De Gouw JA; Brock CA; Gilman J; Lerner BM; Dubé WP; Liao J; Welti A Secondary organic aerosol (SOA) yields from NO3 radical + isoprene based on nighttime aircraft power plant plume transects. Atmospheric Chemistry and Physics 2018, 18, 11663–11682.

(36). Pankow JF; Asher WE SIMPOL.1: A simple group contribution method for predicting vapor pressures and enthalpies of vaporization of multifunctional organic compounds. Atmospheric Chemistry and Physics 2008, 8, 2773–2796.

(37). Nault BA; Campuzano-jost P; Day DA; Schroder JC; Anderson B; Beyersdorf AJ; Blake DR; Brune WH; Choi Y; Corr CA; Kim MJ; Knote CJ; Lamb KD; Lee T; Park T; Pusede SE Secondary organic aerosol production from local emissions dominates the organic aerosol budget over Seoul, South Korea, during KORUS-AQ. Atmospheric Chemistry and Physics 2018, 18, 17769–17800.

(38). Jordan CE; Crawford JH; Beyersdorf AJ; Eck TF; Halliday HS; Nault BA; Chang L-S; Park J; Park R; Lee G; Kim H; Ahn J.-y.; Cho S; Shin HJ; Lee JH; Jung J; Kim D-S; Lee M; Lee T; Whitehill A; Szykman J; Schueneman MK; Campuzano-Jost P; Jimenez JL; DiGangi JP; Diskin GS; Anderson BE; Moore RH; Ziemba LD; Fenn MA; Hair JW; Kuehn RE; Holz RE; Chen G; Travis K; Shook M; Peterson DA; Lamb KD; Schwarz JP Investigation of factors controlling

PM2.5 variability across the South Korean Peninsula during KORUS-AQ. Elementa: Science of the Anthropocene 2020, 8.

(39). Crawford JH; Ahn J-Y; Al-Saadi J; Chang L; Emmons LK; Kim J; Lee G; Park J-H; Park RJ; Woo JH; Song C-K; Hong J-H; Hong Y-D; Lefer BL; Lee M; Lee T; Kim S; Min K-E; Yum SS; Shin HJ; Kim Y-W; Choi J-S; Park J-S; Szykman JJ; Long RW; Jordan CE; Simpson IJ; Fried A; Dibb JE; Cho S; Kim YP The Korea–United States Air Quality (KORUS-AQ) field study. Elementa: Science of the Anthropocene 2021, 9, 1–27.

(40). Park M.-s.; Park S.-h.; Chae J.-h.; Choi M.-h.; Song Y; Kang M High-resolution urban observation network for user-specific meteorological information service in the Seoul Metropolitan Area , South Korea. Atmospheric Measurement Techniques 2017, 10, 1575–1594.

(41). Kim HC; Kim E; Bae C; Cho JH; Kim B-u.; Kim, S. Regional contributions to particulate matter concentration in the Seoul metropolitan area , South Korea : seasonal variation and sensitivity to meteorology and emissions inventory. Atmospheric Chemistry and Physics 2017, 17, 10315–10332.

(42). Fried A; Walega J; Weibring P; Richter D; Simpson IJ; Blake DR; Blake NJ; Meinardi S; Barletta B; Hughes SC; Crawford JH; Diskin G; Barrick J; Hair J; Fenn M; Wisthaler A; Mikoviny T; Woo J-H; Park M; Kim J; Min K-E; Jeong S; Wennberg PO; Kim MJ; Crounse JD; Teng AP; Bennett R; Yang-Martin M; Shook MA; Huey G; Tanner D; Knote C; Kim J; Park R; Brune W Airborne formaldehyde and volatile organic compound measurements over the Daesan petrochemical complex on Korea's northwest coast during the Korea-United States Air Quality study. Elementa: Science of the Anthropocene 2020, 8, 1–28.

(43). Lee BH; Lopez-Hilfiker FD; Mohr C; Kurtén T; Worsnop DR; Thornton JA An iodide-adduct high-resolution time-of-flight chemical-ionization mass spectrometer: Application to atmospheric inorganic and organic compounds. Environmental Science and Technology 2014, 48, 6309–6317. [PubMed: 24800638]

(44). Shi X; Qiu X; Cheng Z; Chen Q; Rudich Y; Zhu T Isomeric Identification of Particle-Phase Organic Nitrates through Gas Chromatography and Time-of-Flight Mass Spectrometry Coupled with an Electron Capture Negative Ionization Source. Environmental Science and Technology 2020, 54 , 707–713. [PubMed: 31865702]

(45). Day DA; Wooldridge PJ; Dillon MB; Thornton JA; Cohen RC A thermal dissociation laser-induced fluorescence instrument for in situ detection of NO2, peroxy nitrates, alkyl nitrates, and HNO3. Journal of Geophysical Research: Atmospheres 2002, 107, 4–1.

(46). Wooldridge PJ; Perring AE; Bertram TH; Flocke FM; Roberts JM; Singh HB; Huey LG; Thornton JA; Wolfe GM; Murphy JG; Fry JL; Rollins AW; Lafranchi BW; Cohen RC Total Peroxy Nitrates (ΣPNs) in the atmosphere: The Thermal Dissociation-Laser Induced Fluorescence (TD-LIF) technique and comparisons to speciated PAN measurements. Atmospheric Measurement Techniques 2010, 3, 593–607.

(47). Rollins AW; Smith JD; Wilson KR; Cohen RC Real time in situ detection of organic nitrates in atmospheric aerosols. Environmental science & technology 2010, 44, 5540–5545. [PubMed: 20575535]

(48). Womack CC; Neuman JA; Veres PR; Eilerman SJ; Brock CA; Decker ZCJ; Zarzana KJ; Dube WP; Wild RJ; Wooldridge PJ; Cohen RC; Brown SS Evaluation of the accuracy of thermal dissociation CRDS and LIF techniques for atmospheric measurement of reactive nitrogen species. Atmospheric Chemistry and Physics 2017, 1911–1926.

(49). Friedrich N; Tadic I; Schuladen J; Brooks J; Darbyshire E; Drewnick F; Fischer H; Lelieveld J; Crowley JN; Crowley JN Measurement of NOxand NOy-with a thermal dissociation cavity ring-down spectrometer (TD-CRDS): Instrument characterisation and first deployment. Atmospheric Measurement Techniques 2020, 13, 5739–5761.

(50). Wiedensohler A An approximation of the bipolar charge distribution for particles in the submicron size range. Journal of Aerosol Science 1988, 19, 387–389.

(51). DeCarlo PF; Kimmel JR; Trimborn A; Northway MJ; Jayne JT; Aiken AC; Gonin M; Fuhrer K; Horvath T; Docherty KS; Worsnop DR; Jimenez JL Field-deployable, high-resolution, time-of-flight aerosol mass spectrometer. Analytical Chemistry 2006, 78, 8281–8289. [PubMed: 17165817]

(52). Canagaratna M; Jayne J; Jimenez J; Allan J; Alfarra M; Zhang Q; Onasch T; Drewnick F; Coe H; Middlebrook A; Delia A; Williams L; Trimborn A; Northway M; DeCarlo PF; Kolb CE; Davidovits P; Worsnop D Chemical and Microphysical Characterization of Ambien Aerosols with the Aerodyne Aerosol Mass Spectrometer. Mass Spectrometry Reviews 2007, 26, 185–222. [PubMed: 17230437]

(53). Farmer DK; Matsunaga A; Docherty KS; Surratt JD; Seinfeld JH; Ziemann PJ; Jimenez JL Response of an aerosol mass spectrometer to organonitrates and organosulfates and implications for atmospheric chemistry. Proceedings of the National Academy of Sciences of the United States of America 2010, 107, 6670–6675. [PubMed: 20194777]

(54). Xu L; Suresh S; Guo H; Weber RJ; Ng NL Aerosol characterization over the southeastern United States using high-resolution aerosol mass spectrometry: Spatial and seasonal variation of aerosol composition and sources with a focus on organic nitrates. Atmospheric Chemistry and Physics 2015, 15, 7307–7336.

(55). Wyat Appel K; Napelenok S; Hogrefe C; Pouliot G; Foley KM; Roselle SJ; Pleim JE; Bash J; Pye HO; Heath N; Murphy B; Mathur R Overview and evaluation of the community multiscale air quality (CMAQ) modeling system version 5.2. Springer Proceedings in Complexity 2018, 69–73.

(56). Kelly JT; Koplitz SN; Baker KR; Holder AL; Pye HO; Murphy BN; Bash JO; Henderson BH; Possiel NC; Simon H; Eyth AM; Jang C; Phillips S; Timin B Assessing PM2.5 model performance for the conterminous U.S. with comparison to model performance statistics from 2007-2015. Atmospheric Environment 2019, 214, 116872.

(57). Zare A; Romer PS; Nguyen T; Keutsch FN; Skog K; Cohen RC A comprehensive organic nitrate chemistry: Insights into the lifetime of atmospheric organic nitrates. Atmospheric Chemistry and Physics 2018, 18, 15419–15436.

(58). Otte TL; Pleim JE The Meteorology-Chemistry Interface Processor (MCIP) for the CMAQ modeling system: Updates through MCIPv3.4.1. Geoscientific Model Development 2010, 3, 243–256.

(59). Woo JH; Kim Y; Kim HK; Choi KC; Eum JH; Lee JB; Lim JH; Kim J; Seong M Development of the CREATE inventory in support of integrated climate and air quality modeling for Asia. Sustainability (Switzerland) 2020, 12.

(60). Guenther AB; Jiang X; Heald CL; Sakulyanontvittaya T; Duhl T; Emmons LK; Wang X Model Development The Model of Emissions of Gases and Aerosols from Nature version 2.1 (MEGAN2. 1): an extended and updated framework for modeling biogenic emissions. Geoscientific Model Development 2012, 5, 1471–1492.

(61). Wiedinmyer C; Akagi SK; Yokelson RJ; Emmons LK; Orlando JJ; Soja AJ Model Development The Fire INventory from NCAR (FINN): a high resolution global model to estimate the emissions from open burning. Geoscientific Model Development 2011, 4, 625–641.

(62). Houyoux MR; Vukovich JM; Coats CJ; Wheeler NJ; Kasibhatla PS Emission inventory development and processing for the Seasonal Model for Regional Air Quality (SMRAQ) project. Journal of Geophysical Research Atmospheres 2000, 105, 9079–9090.

(63). Simpson IJ; Blake DR; Blake NJ; Meinardi S; Barletta B; Hughes SC; Fleming LT; Crawford JH; Diskin GS; Emmons LK; Fried A; Guo H; Peterson DA; Wisthaler A; Woo J-H; Barré J; Gaubert B; Kim J; Kim MJ; Kim Y; Knote C; Mikoviny T; Pusede SE; Schroeder JR; Wang Y; Wennberg PO; Zeng L Characterization, sources and reactivity of volatile organic compounds (VOCs) in Seoul and surrounding regions during KORUS-AQ. Elementa: Science of the Anthropocene 2020, 8.

(64). McDonald BC; De Gouw JA; Gilman JB; Jathar SH; Akherati A; Cappa CD; Jimenez JL; Lee-Taylor J; Hayes PL; McKeen SA; Cui YY; Kim SW; Gentner DR; Isaacman-VanWertz G; Goldstein AH; Harley RA; Frost GJ; Roberts JM; Ryerson TB; Trainer M Volatile chemical products emerging as largest petrochemical source of urban organic emissions. Science 2018, 359, 760–764. [PubMed: 29449485]

(65). Gkatzelis GI; Coggon MM; McDonald BC; Peischl J; Aikin KC; Gilman JB; Trainer M; Warneke C Identifying Volatile Chemical Product Tracer Compounds in U.S. Cities. Environmental Science and Technology 2021, 55, 188–199. [PubMed: 33325693]

(66). Crounse JD; McKinney KA; Kwan AJ; Wennberg PO Measurement of gas-phase hydroperoxides by chemical ionization mass spectrometry. Analytical Chemistry 2006, 78, 6726–6732. [PubMed: 17007490]

(67). Goliff WS; Stockwell WR; Lawson CV The regional atmospheric chemistry mechanism, version 2. Atmospheric Environment 2013, 68, 174–185.

(68). Sarwar G; Godowitch J; Henderson BH; Fahey K; Pouliot G; Hutzell WT; Mathur R; Kang D A comparison of atmospheric composition using the Carbon Bond and Regional Atmospheric Chemistry Mechanisms. Atmospheric Chemistry and Physics 2013, 13, 9695–9712.

(69). Browne EC; Wooldridge PJ; Min K; Cohen RC On the role of monoterpene chemistry in the remote continental boundary layer. Atmospheric Chemistry and Physics 2014, 14, 1225–1238.

(70). Carter WP; Atkinson R Alkyl Nitrate Formation from the Atmospheric Photooxidation of Alkanes; a Revised Estimation Method. Journal of Atmospheric Chemistry 1989, 8, 165–173.

(71). Middleton P; Stockwell WR; Carter WP Aggregation and analysis of volatile organic compound emissions for regional modeling. Atmospheric Environment Part A, General Topics 1990, 24, 1107–1133.

(72). Arey J; Aschmann SM; Kwok ES; Atkinson R Alkyl Nitrate, Hydroxyalkyl Nitrate, and Hydroxycarbonyl Formation from the NOx - Air Photooxidations of C5-C8 w-ALkanes. Journal of Physical Chemistry A 2001, 105, 1020–1027.

(73). Jenkin ME; Saunders SM; Pilling MJ The tropospheric degradation of volatile organic compounds: a protocol for mechanism development. Atmospheric Environment 1997, 31, 81–104.

(74). Saunders SM; Jenkin ME; Derwent RG; Pilling MJ Protocol for the development of the Master Chemical Mechanism, MCM v3 (Part A): tropospheric degradation of non-aromatic volatile organic compounds. Atmospheric Chemistry and Physics 2003, 3, 161–180.

(75). Leungsakul S; Jeffries HE; Kamens RM A kinetic mechanism for predicting secondary aerosol formation from the reactions of d-limonene in the presence of oxides of nitrogen and natural sunlight. Atmospheric Environment 2005, 39, 7063–7082.

(76). Spittler M; Barnes I; Bejan I; Brockmann KJ; Benter T; Wirtz K Reactions of NO3 radicals with limonene and α-pinene: Product and SOA formation. Atmospheric Environment 2006, 40, 116–127.

(77). Paulot F; Crounse JD; Kjaergaard HG; Kroll JH; Seinfeld JH; Wennberg PO Isoprene photooxidation: new insights into the production of acids and organic nitrates. Atmospheric Chemistry and Physics 2009, 9, 1479–1501.

(78). Paulot F; Crounse JD; Kjaergaard HG; Kürten A; Clair JMS; Seinfeld JH; Wennberg PO Unexpected Epoxide Formation in the Gas-Phase Photooxidation of Isoprene. Science 2009, 325, 730–734. [PubMed: 19661425]

(79). Crounse JD; Paulot F; Kjaergaard G; Wennberg PO Peroxy radical isomerization in the oxidation of isoprene. Physical Chemistry Chemical Physics 2011, 13607–13613. [PubMed: 21701740]

(80). Ng NL; Brown SS; Archibald AT; Atlas E; Cohen RC; Crowley JN; Day DA; Donahue NM; Fry JL; Fuchs H; Griffin RJ; Guzman MI; Herrmann H; Hodzic A; Iinuma Y; Kiendler-Scharr A; Lee BH; Luecken DJ; Mao J; McLaren R; Mutzel A; Osthoff HD; Ouyang B; Picquet-Varrault B; Platt U; Pye HO; Rudich Y; Schwantes RH; Shiraiwa M; Stutz J; Thornton JA; Tilgner A; Williams BJ; Zaveri RA Nitrate radicals and biogenic volatile organic compounds: Oxidation, mechanisms, and organic aerosol. Atmospheric Chemistry and Physics 2017, 17, 2103–2162. [PubMed: 30147712]

(81). Xu ZN; Nie W; Chi XG; Sun P; Huang DD; Yan C; Krechmer J; Ye PL; Xu Z; Qi XM; Zhu C; Liu YL; Li YY; Wang TY; Wang L; Huang X; Tang RZ; Guo S; Xiu GL; Fu QY; Worsnop D; Ding AJ Multifunctional products of isoprene oxidation in polluted atmosphere and their contribution to SOA. Geophysical Research Letters 2020, 1–10.

(82). Donahue NM; Robinson AL; Stanier CO; Pandis SN Coupled partitioning, dilution, and chemical aging of semivolatile organics. Environmental Science and Technology 2006, 40, 2635–2643. [PubMed: 16683603]

(83). Pankow JF An absorption model of the gas/aerosol partitioning involved in the formation of secondary organic aerosol. Atmospheric Environment 1994, 28, 189–193.

(84). Epstein SA; Riipinen I; Donahue NM A semiempirical correlation between enthalpy of vaporization and saturation concentration for organic aerosol. Environmental Science and Technology 2010, 44, 743–748. [PubMed: 20025284]

(85). Park RJ; Oak YJ; Emmons LK; Kim CH; Pfister GG; Carmichael GR; Saide PE; Cho SY; Kim S; Woo JH; Crawford JH; Gaubert B; Lee HJ; Park SY; Jo YJ; Gao M; Tang B; Stanier CO; Shin SS; Park HY; Bae C; Kim E Multi-model intercomparisons of air quality simulations for the KORUS-AQ campaign. Elementa 2021, 9, 1–29. [PubMed: 34926709]

(86). Robinson AL; Donahue NM; Shrivastava MK; Weitkamp EA; Sage AM; Grieshop AP; Lane TE; Pierce JR; Pandis SN Rethinking organic aerosols: Semivolatile emissions and photochemical aging. Science 2007, 315, 1259–1262. [PubMed: 17332409]

(87). Grieshop AP; Logue JM; Donahue NM; Robinson AL Laboratory investigation of photochemical oxidation of organic aerosol from wood fires 1: Measurement and simulation of organic aerosol evolution. Atmospheric Chemistry and Physics 2009, 9, 1263–1277.

(88). Dzepina K; Volkamer RM; Madronich S; Tulet P; Ulbrich IM; Zhang Q; Cappa CD; Ziemann PJ; Jimenez JL Evaluation of recently-proposed secondary organic aerosol models for a case study in Mexico City. Atmospheric Chemistry and Physics 2009, 9, 5681–5709.

(89). Hodzic A; Jimenez JL; Madronich S; Canagaratna MR; Decarlo PF; Kleinman L; Fast J Modeling organic aerosols in a megacity: Potential contribution of semi-volatile and intermediate volatility primary organic compounds to secondary organic aerosol formation. Atmospheric Chemistry and Physics 2010, 10, 5491–5514.

(90). Pye HO; Seinfeld JH A global perspective on aerosol from low-volatility organic compounds. Atmospheric Chemistry and Physics 2010, 10, 4377–4401.

(91). Dzepina K; Cappa CD; Volkamer RM; Madronich S; Decarlo PF; Zaveri RA; Jimenez JL Modeling the multiday evolution and aging of secondary organic aerosol during MILAGRO 2006. Environmental Science and Technology 2011, 45, 3496–3503 [PubMed: 21425791]

(92). Zhao Y; Hennigan CJ; May AA; Tkacik DS; De Gouw JA; Gilman JB; Kuster WC; Borbon A; Robinson AL Intermediate-volatility organic compounds: A large source of secondary organic aerosol. Environmental Science and Technology 2014, 48, 13743–13750. [PubMed: 25375804]

(93). Ortega AM; Hayes PL; Peng Z; Palm BB; Hu W; Day DA; Li R; Cubison MJ; Brune WH; Graus M; Warneke C; Gilman JB; Kuster WC; De Gouw J; Gutiérrez-Montes C; Jimenez JL Real-time measurements of secondary organic aerosol formation and aging from ambient air in an oxidation flow reactor in the Los Angeles area. Atmospheric Chemistry and Physics 2016, 16, 7411–7433.

(94). Pagonis D; Krechmer JE; De Gouw J; Jimenez JL; Ziemann PJ Effects of gas-wall partitioning in Teflon tubing and instrumentation on time-resolved measurements of gas-phase organic compounds. Atmospheric Measurement Techniques 2017, 10, 4687–4696.

(95). Zhang X; Cappa CD; Jathar SH; McVay RC; Ensberg JJ; Kleeman MJ; Seinfeld JH Influence of vapor wall loss in laboratory chambers on yields of secondary organic aerosol. Proceedings of the National Academy of Sciences of the United States of America 2014, 111, 5802–5807. [PubMed: 24711404]

(96). Crounse JD; Nielsen LB; Jørgensen S; Kjaergaard HG; Wennberg PO Autoxidation of organic compounds in the atmosphere. Journal of Physical Chemistry Letters 2013, 4, 3513–3520.

(97). Bianchi F; Kurtén T; Riva M; Mohr C; Rissanen MP; Roldin P; Berndt T; Crounse JD; Wennberg PO; Mentel TF; Wildt J; Junninen H; Jokinen T; Kulmala M; Worsnop DR; Thornton JA; Donahue N; Kjaergaard HG; Ehn M Highly Oxygenated Organic Molecules (HOM) from Gas-Phase Autoxidation Involving Peroxy Radicals: A Key Contributor to Atmospheric Aerosol. Chemical Reviews 2019, 119, 3472–3509. [PubMed: 30799608]

(98). Tröstl J; Chuang WK; Gordon H; Heinritzi M; Yan C; Molteni U; Ahlm L; Frege C; Bianchi F; Wagner R; Simon M; Lehtipalo K; Williamson C; Craven JS; Duplissy J; Adamov A; Almeida J; Bernhammer AK; Breitenlechner M; Brilke S; Dias A; Ehrhart S; Flagan RC; Franchin A; Fuchs C; Guida R; Gysel M; Hansel A; Hoyle CR; Jokinen T; Junninen H; Kangasluoma J; Keskinen H; Kim J; Krapf M; Kürten A; Laaksonen A; Lawler M; Leiminger M; Mathot S; Möhler O; Nieminen T; Onnela A; Petäjä T; Piel FM; Miettinen P; Rissanen MP; Rondo L; Sarnela N; Schobesberger S; Sengupta K; Sipilä M; Smith JN; Steiner G; Tomè A; Virtanen A; Wagner AC; Weingartner E; Wimmer D; Winkler PM; Ye P; Carslaw KS; Curtius J; Dommen J; Kirkby J; Kulmala M; Riipinen I; Worsnop DR; Donahue NM; Baltensperger U The role of low-volatility

organic compounds in initial particle growth in the atmosphere. Nature 2016, 533, 527–531. [PubMed: 27225126]

(99). Ehn M; Thornton JA; Kleist E; Sipilä M; Junninen H; Pullinen I; Springer M; Rubach F; Tillmann R; Lee B; Lopez-Hilfiker F; Andres S; Acir IH; Rissanen M; Jokinen T; Schobesberger S; Kangasluoma J; Kontkanen J; Nieminen T; Kurtén T; Nielsen LB; Jørgensen S; Kjaergaard HG; Canagaratna M; Maso MD; Berndt T; Petäjä T; Wahner A; Kerminen VM; Kulmala M; Worsnop DR; Wildt J; Mentel TF A large source of low-volatility secondary organic aerosol. Nature 2014, 506, 476–479. [PubMed: 24572423]

(100). Mutzel A; Poulain L; Berndt T; Iinuma Y; Rodigast M; Böge O; Richters S; Spindler G; Sipilä M; Jokinen T; Kulmala M; Herrmann H Highly Oxidized Multifunctional Organic Compounds Observed in Tropospheric Particles: A Field and Laboratory Study. Environmental Science and Technology 2015, 49, 7754–7761. [PubMed: 26011767]

(101). Pye HO; D'Ambro EL; Lee BH; Schobesberger S; Takeuchi M; Zhao Y; Lopez-Hilfiker F; Liu J; Shilling JE; Xing J; Mathur R; Middlebrook AM; Liao J; Welti A; Graus M; Warneke C; de Gouw JA; Holloway JS; Ryerson TB; Pollack IB; Thornton JA Anthropogenic enhancements to production of highly oxygenated molecules from autoxidation. Proceedings of the National Academy of Sciences of the United States of America 2019, 116, 6641–6646. [PubMed: 30886090]

(102). Wang S; Wu R; Berndt T; Ehn M; Wang L Formation of Highly Oxidized Radicals and Multifunctional Products from the Atmospheric Oxidation of Alkylbenzenes. Environmental Science and Technology 2017, 51, 8442–8449. [PubMed: 28682596]

(103). Tsiligiannis E; Hammes J; Salvador CM; Mentel T; Hallquist M Effect of NOx on 1,3,5-trimethylbenzene (TMB) oxidation product distribution and particle formation. Atmospheric Chemistry and Physics 2019, 19, 15073–15086.

(104). Garmash O; Rissanen MP; Pullinen I; Schmitt S; Kausiala O; Tillmann R; Zhao D; Percival C; Bannan TJ; Priestley M; Hallquist AM; Kleist E; Kiendler-Scharr A; Hallquist M; Berndt T; McFiggans G; Wildt J; Mentel TF; Ehn M Multi-generation OH oxidation as a source for highly oxygenated organic molecules from aromatics. Atmospheric Chemistry and Physics 2020, 20, 515–537.

(105). Cheng X; Chen Q; Li YJ; Zheng Y; Liao K; Huang G Highly Oxygenated Organic Molecules Produced by the Oxidation of Benzene and Toluene in a Wide Range of OH Exposure and NOx Conditions. Atmospheric Chemistry and Physics 2021, 12005–12019.

Synopsis:

We use aircraft-based measurements and modeling to explore the organic nitrate aerosol in Korea as a model for cities worldwide.

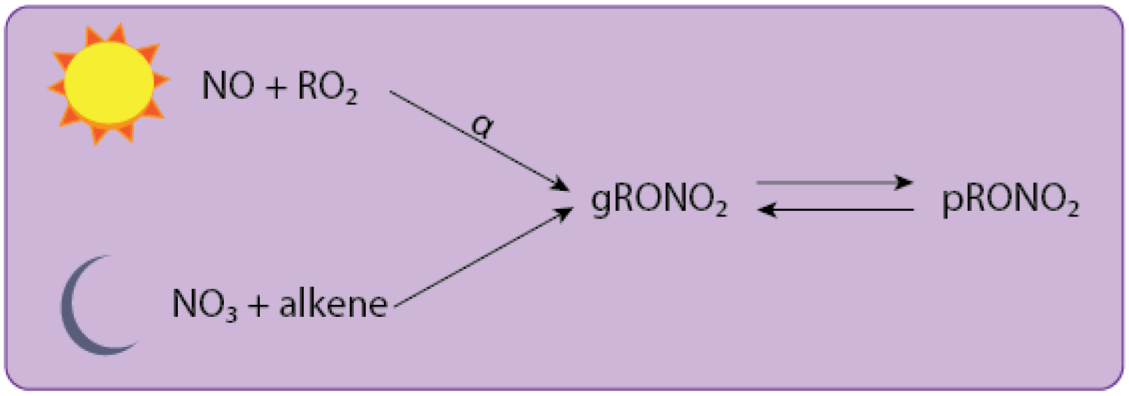

Figure 1:
Schematic of $RONO_2$ production and phase partitioning.

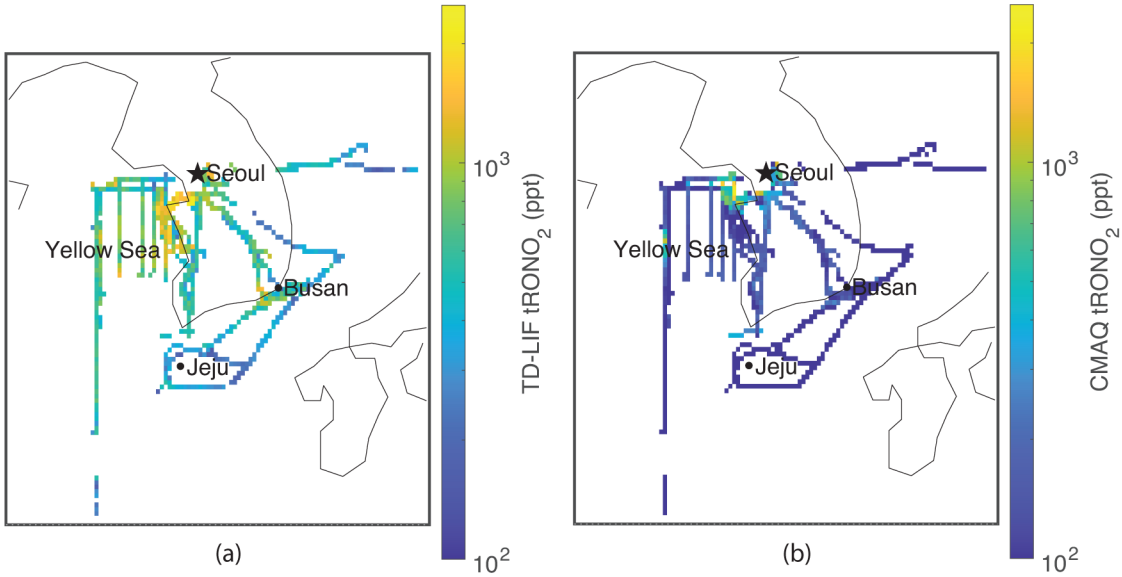

Figure 2:

Maps of average (a) TD-LIF measured and (b) CMAQ modeled $tRONO_2$ on a log scale, gridded to 0.1°. Seoul, Jeju, Busan, and the Yellow Sea are labeled for reference. Note the modeling domain is larger than the domain of the map plotted here and covers much of Northeast Asia (17.4 - 47.2°N and 93.2-147.4°E).

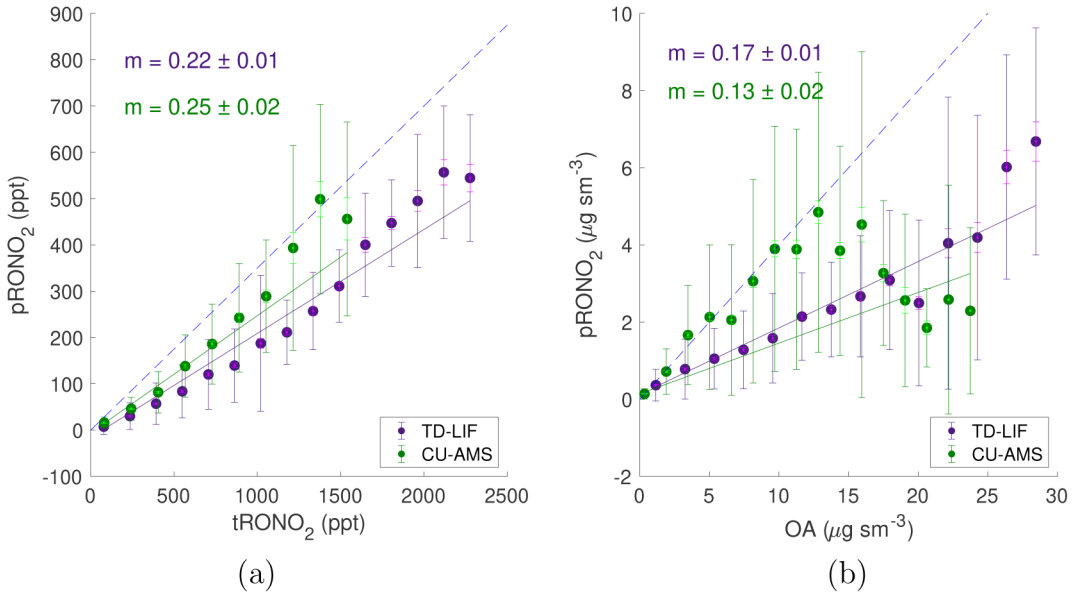

Figure 3:

(a) Plot of $pRONO_2$ versus $tRONO_2$ mixing ratios as measured by TD-LIF and CU-AMS. Data are binned by $tRONO_2$ mixing ratio, and the average $pRONO_2$ in each bin is plotted. The York fit shown corresponds to the average fraction of $RONO_2$ in the particle phase (F_p). We draw an estimated upper limit (≈35%) for the fraction of $RONO_2$ in the particle phase, as shown in the blue dashed line, drawn above the mean of most measurements. (b) Plot of $pRONO_2$ mass concentration (using an estimated average molecular weight of 300 g mol^{-1}) versus OA mass concentration. Data are binned by OA concentration, and the average $pRONO_2$ in each bin is plotted. The York fit shown corresponds to the average fraction OA mass that can be attributed to $pRONO_2$. Again, we draw an estimated upper limit (≈40%) for the fraction of OA mass attributable to $pRONO_2$, as shown in the blue dashed line, drawn above most measurement means. We do not understand why AMS data above 15 μg m^{-3} deviates so strongly from the trend measured at lower OA concentrations. In both plots, the larger, dark colored error bars correspond to the standard deviation of measurements within each bin to represent observed variability whereas the smaller, light colored error bars correspond to the standard error of measurements within each bin to represent measurement uncertainty. We apply a threshold requirement of 20 observations per bin to include in plot.

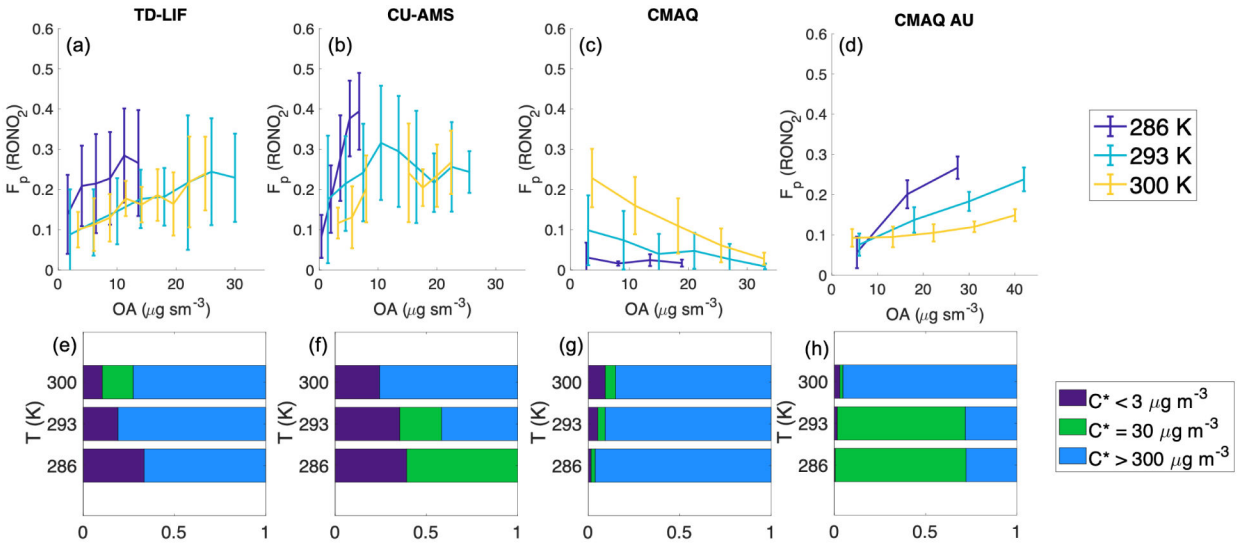

Figure 4:

[Top] Plots of the fraction of $RONO_2$ in the particle phase (F_p) versus OA concentration. Data were separated into three temperature bins (centered at 286, 293, and 300 K) and binned by OA concentration. The average F_p in each OA bin is plotted, and error bars represent the standard deviation of F_p in each bin. As suggested by absorptive partitioning theory, measured F_p increases with increasing available solvating aerosol (in this case, OA). [Bottom] Temperature-dependent fractional distribution (f_j) of saturation concentrations (C_j^*) fit to a volatility basis set. Each set of plots is shown for the TD-LIF measurements (a,e), the CU-AMS measurements (b,f), unmodified CMAQ output (c,g), and CMAQ output with an unknown source of $RONO_2$ added (d,h).

Table 1:

Comparison of the York fit slopes between measured (TD-LIF and CU-AMS) and CMAQ modeled concentrations of $tRONO_2$, $pRONO_2$, and F_p. Comparison is shown for both the unmodified CMAQ output and CMAQ output with an unknown source of condensable $RONO_2$ added. Scatter plots of these comparisons can be seen in Figure S14.

	$tRONO_2$		**$pRONO_2$**		**F_p**	
	TD-LIF	**CU-AMS**	**TD-LIF**	**CU-AMS**	**TD-LIF**	**CU-AMS**
CMAQ	0.30	0.35	0.12	0.09	0.56	0.35
CMAQ add unknown	0.88	0.98	0.92	0.79	0.61	0.44